Table 1 Alignment of the *HLA-B* sequence and genotype in 96 samples *(Continued)*

1224	HLA-B*40:02	HLA-B*40:03	HLA-B*40:02:01	HLA-B*40:03	6306.5	6286.4	Only 3 heterozygous SNVs
1225	HLA-B*40:01	HLA-B*44:03	HLA-B*40:01:02	HLA-B*44:03:01	1554	1399.6	
1229	HLA-B*52:01	HLA-B*52:01	HLA-B*52:01:01:02	HLA-B*52:01:01:02	6748.5		Homozygous
1234	HLA-B*44:03	HLA-B*40:06	HLA-B*44:03:01	HLA-B*40:06:01:01	2490.3	1715.9	
1236	HLA-B*54:01	HLA-B*40:06	HLA-B*54:01:01	HLA-B*40:06:01:01	1132.4	1244.4	
1238	HLA-B*40:02	HLA-B*67:01	HLA-B*40:02:01	HLA-B*67:01:01	2040.9	1691	
1239	HLA-B*40:03	HLA-B*51:01	HLA-B*40:03	HLA-B*51:01:01	1787	1789.8	
1250	HLA-B*44:03	HLA-B*51:01	HLA-B*44:03:01	HLA-B*51:01:01	357.7	317.8	
1259	HLA-B*40:02	HLA-B*07:02	HLA-B*40:02:01	HLA-B*07:02:01	1346.9	1934.4	
1260	HLA-B*40:06	HLA-B*35:01	HLA-B*40:06:01:01	HLA-B*35:01:01:02	641.9	680.8	
1265	HLA-B*40:01	HLA-B*40:06	HLA-B*40:01:02	HLA-B*40:06:01:01	2226.2	1691.7	

*Phase defined sequencing pipeline.

HLA gene sequencing and typing using an automated system.

Methods

Subjects

A total of 96 unrelated healthy Japanese control subjects were recruited at the Health Evaluation and Promotion Center of Tokai University Hospital. All subjects gave written informed consent for the study. Ethical approvals for this study protocol were obtained from the IRBs of National Institute of Genetics and Tokai University School of Medicine.

DNA samples

DNA samples were extracted from peripheral blood using a DNA extraction kit Genomix (Biologica, Nagoya, Japan) using the manufacturer's instructions.

HLA genotyping with PCR-SSO method

We genotyped *HLA-B* using the Luminex assay system and HLA typing kits (WAKFlow HLA Typing kits, Wakunaga, Osaka, Japan or LABType SSO, One Lambda, Canoga Park, CA, USA).

Library preparation

HLA-B was amplified using locus-specific primers by long-range PCR [1]. Each amplification reaction contained 20 ng of genomic DNA, 0.25 unit of PrimeSTAR® GXL DNA polymerase (TAKARA BIO Inc., Shiga, Japan), 1× PrimeSTAR® GXL buffer (Mg^{2}+ concentration 1 mM), 0.2 mM of each dNTP, and 0.2 μM of each primer in a 10 μl reaction volume. Cycling parameters were as follows: initial denaturation of 94°C for 2 min followed by 30 cycles of 98°C for 10 s, 60°C for 15 s, and 68°C for 5 min. Each PCR product concentration was measured with a Qubit dsDNA BR Assay Kit (Life Technologies, Carlsbad, CA, USA). PCR products were subjected to library preparation with a Nextera DNA Sample Preparation Kit (Illumina, San Diego, CA, USA) and a KAPA Library Amplification kit (Kapa Biosystems, Inc., Wilmington, MA, USA). The KAPA kit was used for library amplification because of its advantage of coverage depth in high-GC-content regions during library amplification (Additional file 5: Figure S5). Each sample was dual indexed and normalized with modified AMPure XP beads (Beckman Coulter Inc., Brea, CA, USA) method, which include optimal size selection and normalization of DNA concentration (Figure 1).

BeNUS for 96-well plate-based library

We prepared altered AMPure XP beads by resuspending the beads in half of the original volume of 20% polyethylene glycol 8000 (PEG) and 2.5 M NaCl solution. The resuspended beads were twice as concentrated as the standard AMPure XP beads (Additional file 6: Figure S6). The optimal volume ratio of altered beads to DNA solution was determined by relation between the PEG–NaCl concentration and the selected DNA fragment size (Additional file 6: Figure S6). For library size selection, 20 μl of resuspended altered beads was added to 50 μl of diluted library (5 μl of PCR product and 45 μl of water), mixed well by pipetting at least 10 times, and incubated for 5 min at room temperature. The tube was placed on the NGS MagnaStand (NIPPON Genetics, Tokyo, Japan) to separate the beads from the supernatant. After separation, the supernatant was carefully transferred to a new tube. Five μl of the altered beads were added to the supernatant, mixed, and incubated, and the beads were then separated from the supernatant on the same conditions. The supernatant containing unwanted DNA was carefully removed. One hundred μl of 80% ethanol was added to the tube for washing and the supernatant was carefully discarded after incubation and separation. The beads were air-dried for 10 min while the tube was on the magnetic

stand with the lid open. The target library was eluted from the beads into 22 μl of water (Figure 1). Next, to normalize DNA concentration, altered beads, which were diluted 20 fold with 20% PEG and 2.5 M NaCl solution, were used to capture a certain amount of DNA (Additional file 2: Figure S2). Twenty μl of 20-fold diluted altered beads and 20 μl of isopropanol were added to the 20 μl of size-selected library, mixed well by pipetting at least 10 times, and incubated for 5 min at room temperature. The tube was placed on the magnetic stand to separate the beads from the supernatant. After the supernatant was discarded, 100 μl of 80% ethanol was added to the tube kept on the magnetic stand and incubated at room temperature for 30 s, and then the supernatant was carefully discarded. The beads were air-dried, and then 20 μl of water was added to elute the normalized libraries (Figure 1). The combination of fragment size selection and normalization of DNA amount results in an equalized DNA molar concentration among 96 libraries.

Sequencing

Equal volumes of libraries were pooled and subjected to multiplex sequencing on the MiSeq sequencer (Illumina). The MiSeq flow cell of 2 × 300 bp paired-end reads resulted in 11.6 million read pairs corresponding to 6 Gbp of valid sequence data without adapter sequence.

Determination of the *HLA-B* sequence

Sequence reads were distributed according to index information to assign samples. We used the phase-defined sequencing pipeline (http://p-galaxy.ddbj.nig.ac.jp) [1,10], which include trimming low quality bases (Phred quality score < Q20), selection of only long (>200 bp) paired-end reads, alignment to reference sequence, SNVs and indel identification, and haplotype phasing. *HLA-B* sequence (UCSC hg19, chr6: 31,317,316 – 31,331,864, complement) was used as reference sequence. After phasing, two BAM files were created as phased *HLA-B* alignments. The IGV genome viewer [11] was used to visualize the alignment results. The consensus sequences in FASTQ or FASTA format were constructed for searching the IMGT/HLA (http://www.ebi.ac.uk/imgt/hla/) database to identify the HLA alleles. We used them as query for BLAT [12] search to known HLA allele sequences in the database as complete matches of genomic sequence or CDS sequence. For validation, *HLA-B* genotype calls were compared with the result of PCR-SSO and Omixon Target HLA Typing (Omixon Inc., Budapest, Hungary) [13,14].

Availability of supporting data

The data set associated with this project has been submitted to DDBJ Sequence Reads Archive (DRA accession number: DRA001289).

Additional files

Additional file 1: Figure S1. Fragment size selection focusing on the 500–1,000 bp size range.

Additional file 2: Figure S2. Association between number of beads and bound DNA for normalization of DNA concentration.

Additional file 3: Figure S3. Effect of DNA normalization as confirmed by BioAnalyzer.

Additional file 4: Figure S4. Example of partial phasing for a specific exon.

Additional file 5: Figure S5. KAPA Library Amplification kit showing high coverage in a high-GC-content region.

Additional file 6: Figure S6. Method for preparation of beads and optimal bead volume in the DNA solution.

Competing interests

The authors declare that they have no competing interests.

Authors' contributions

KH and II designed the research and prepared the manuscript. KH and HN developed the bioinformatics method. SM performed HLA typing using the SSO method. All authors read and approved the final manuscript.

Acknowledgements

This work was supported by MEXT KAKENHI Grant Numbers 22133002 and 221S0002 (K.H, I.I). We are grateful to Mr. Masayuki Tanaka, the Education and Research Support Center, Research and Development Division, Isehara, Tokai University, and Dr. Yasukazu Nakamura and Dr. Eli Kaminuma, Center for Information Biology and DNA Data Bank of Japan, National Institute of Genetics for their *in silico* work, and Dr. Timothy A. Jinam, Division of Human Genetics, National Institute of Genetics, for comments on our manuscript. We express our deepest gratitude to Mr. Ryota Sugimoto, Ms. Junko Kajiwara, and Ms. Yuko Okudaira for their technical assistance.

Author details

[1]Division of Human Genetics, National Institute of Genetics, 1111 Yata, Mishima, 411-8540 Shizuoka, Japan. [2]Department of Molecular Life Sciences, Tokai University School of Medicine, 143 Shimokasuya, 259-1143 Isehara, Kanagawa, Japan. [3]Genome Informatics Laboratory, Center for Information Biology and DNA Data Bank of Japan, National Institute of Genetics, 1111 Yata, Mishima, 411-8540 Shizuoka, Japan.

Received: 28 January 2014 Accepted: 30 July 2014
Published: 4 August 2014

References

1. Hosomichi K, Jinam TA, Mitsunaga S, Nakaoka H, Inoue I: **Phase-defined complete sequencing of the HLA genes by next-generation sequencing.** *BMC Genomics* 2013, **14**:355.
2. Bentley G, Higuchi R, Hoglund B, Goodridge D, Sayer D, Trachtenberg EA, Erlich HA: **High-resolution, high-throughput HLA genotyping by next-generation sequencing.** *Tissue Antigens* 2009, **74**:393–404.
3. Lind C, Ferriola D, Mackiewicz K, Heron S, Rogers M, Slavich L, Walker R, Hsiao T, McLaughlin L, D'Arcy M, Gai X, Goodridge D, Sayer D, Monos D: **Next-generation sequencing: the solution for high-resolution, unambiguous human leukocyte antigen typing.** *Hum Immunol* 2010, **71**:1033–1042.
4. Erlich RL, Jia X, Anderson S, Banks E, Gao X, Carrington M, Gupta N, DePristo MA, Henn MR, Lennon NJ, de Bakker PI: **Next-generation sequencing for HLA typing of class I loci.** *BMC Genomics* 2011, **12**:42.
5. Wang C, Krishnakumar S, Wilhelmy J, Babrzadeh F, Stepanyan L, Su LF, Levinson D, Fernandez-Viña MA, Davis RW, Davis MM, Mindrinos M: **High-throughput, high-fidelity HLA genotyping with deep sequencing.** *Proc Natl Acad Sci U S A* 2012, **109**:8676–8681.
6. Lank SM, Wiseman RW, Dudley DM, O'Connor DH: **A novel single cDNA amplicon pyrosequencing method for high-throughput, cost-effective sequence-based HLA class I genotyping.** *Hum Immunol* 2010, **71**:1011–1017.
7. Lank SM, Golbach BA, Creager HM, Wiseman RW, Keskin DB, Reinherz EL, Brusic V, O'Connor DH: **Ultra-high resolution HLA genotyping and allele**

discovery by highly multiplexed cDNA amplicon pyrosequencing. *BMC Genomics* 2012, **13**:378.
8. Shiina T, Suzuki S, Ozaki Y, Taira H, Kikkawa E, Shigenari A, Oka A, Umemura T, Joshita S, Takahashi O, Hayashi Y, Paumen M, Katsuyama Y, Mitsunaga S, Ota M, Kulski JK, Inoko H: **Super high resolution for single molecule-sequence-based typing of classical HLA loci at the 8-digit level using next generation sequencers.** *Tissue Antigens* 2012, **80**:305–316.
9. Quail MA, Smith M, Coupland P, Otto TD, Harris SR, Connor TR, Bertoni A, Swerdlow HP, Gu Y: **A tale of three next generation sequencing platforms: comparison of Ion Torrent, Pacific Biosciences and Illumina MiSeq sequencers.** *BMC Genomics* 2012, **13**:341.
10. Nagasaki H, Mochizuki T, Kaminuma E, Watanabe S, Morizaki S, Kodama Y, Saruhashi S, Takagi T, Okubo K, Nakamura Y: **DDBJ read annotation pipeline: a cloud computing based pipeline for high-throughput analysis of next generation sequencing data.** *DNA Res* 2013, **20**:383–390.
11. Thorvaldsdóttir H, Robinson JT, Mesirov JP: **Integrative Genomics Viewer (IGV): high-performance genomics data visualization and exploration.** *Brief Bioinform* 2013, **14**:178–192.
12. Kent WJ: **BLAT–the BLAST-like alignment tool.** *Genome Res* 2002, **12**:656–664.
13. Major E, Rigó K, Hague T, Bérces A, Juhos S: **HLA typing from 1000 genomes whole genome and whole exome illumina data.** *PLoS One* 2013, **8**:e78410.
14. Kulski JK, Suzuki S, Ozaki Y, Mitsunaga S, Inoko H, Shiina T: **In phase HLA genotyping by next generation sequencing - a comparison between two massively parallel sequencing bench-top systems, the Roche GS Junior and ion torrent PGM.** In *HLA and Associated Important Diseases.* Edited by Xi Y. 2014:143–181. InTech.

doi:10.1186/1471-2164-15-645
Cite this article as: Hosomichi *et al.*: A Bead-based Normalization for Uniform Sequencing depth (BeNUS) protocol for multi-samples sequencing exemplified by *HLA-B*. *BMC Genomics* 2014 15:645.

Biochemical and Biophysical Research Communications 446 (2014) 857–862

Contents lists available at ScienceDirect

Biochemical and Biophysical Research Communications

journal homepage: www.elsevier.com/locate/ybbrc

Molecular interplays involved in the cellular uptake of octaarginine on cell surfaces and the importance of syndecan-4 cytoplasmic V domain for the activation of protein kinase Cα

Ikuhiko Nakase [a,b,*], Katsuhiro Osaki [a], Gen Tanaka [a], Atsushi Utani [c], Shiroh Futaki [a,*]

[a] Institute for Chemical Research, Kyoto University, Uji, Kyoto 611-0011, Japan
[b] Nanoscience and Nanotechnology Research Center, Research Organization for the 21st Century, Osaka Prefecture University, Naka-ku, Sakai, Osaka 599-8570, Japan
[c] Department of Dermatology, Nagasaki University Graduate School of Biomedical Sciences, 1-7-1 Sakamoto, Nagasaki, Nagasaki 852-8501, Japan

ARTICLE INFO

Article history:
Received 27 February 2014
Available online 12 March 2014

Keywords:
Cell-penetrating peptides
Syndecan-4
PKCα
Macropinocytosis

ABSTRACT

Arginine-rich cell-penetrating peptides (CPPs) are promising carriers for the intracellular delivery of various bioactive molecules. However, many ambiguities remain about the molecular interplays on cell surfaces that ultimately lead to endocytic uptake of CPPs. By treatment of cells with octaarginine (R8), enhanced clustering of syndecan-4 on plasma membranes and binding of protein kinase Cα (PKCα) to the cytoplasmic domain of syndecan-4 were observed; these events potentially lead to the macropinocytic uptake of R8. The cytoplasmic V domain of syndecan-4 made a significant contribution to the cellular uptake of R8, whereas the cytoplasmic C1 and C2 domains were not involved in the process.

1. Introduction

Arginine-rich cell-penetrating peptides (CPPs) such as the human immunodeficiency virus type 1 (HIV-1) Tat (48–60) peptide and oligoarginine peptides are promising carriers for the intracellular delivery of various bioactive molecules. CPPs hold particular promise for carrying molecules that are otherwise difficult for cells to internalize, such as proteins, peptides, and nucleic acids [1,2]. Although a detailed understanding of cellular uptake mechanisms of arginine-rich CPPs should rationally lead to the design of improved delivery systems, efforts to achieve this have been hampered by the involvement of multiple and complicated pathways in the internalization of CPPs into cells, which include physiological cellular uptake (*i.e.*, endocytosis) and direct permeation through the plasma membranes [1,2]. Macropinocytosis (accompanied by actin reorganization, plasma membrane ruffling, and the stimulated engulfment of large volumes of extracellular fluid) [3,4] has been shown to be an important pathway for the physiological cellular uptake of arginine-rich CPPs [5–9]. We previously reported that the accumulation of arginine-rich CPPs at proteoglycans on plasma membranes leads to the activation of Rac1 and induction of macropinocytosis [8]. The induction of macropinocytosis by arginine-rich CPPs is significantly suppressed by a deficiency in glycosaminoglycans (GAGs) in the plasma membrane due to reduced CPP accumulation on cell membranes [8]. The formation of divalent hydrogen bonds and electrostatic interactions between the arginines and sulfates in GAGs are considered important for the accumulation of CPPs on plasma membranes [1].

Syndecans are type I transmembrane heparan sulfate proteoglycans (HSPGs). Syndecan-4 (Syn-4) is expressed on the surface of nearly all cell types, whereas syndecan-1 (epithelial and plasma cells), syndecan-2 (fibroblasts, endothelial cells, smooth muscle cells, and mesenchymal cells), and syndecan-3 (neuronal cells) are expressed on the membranes of specific cell types [10–12]. Syn-4 is an integral membrane protein with attached heparan sulfate chains, which are linear polysaccharides comprised of glucuronic/iduronic acid and glucosamine residues. The Syn-4 core protein is composed of an extracellular domain, a transmembrane region, and a conserved short C-terminal cytoplasmic domain (CD) [10]. The CD harbors structural features that contribute to signal

Abbreviations: CPPs, cell-penetrating peptides; GAGs, glycosaminoglycans; HSPGs, heparan sulfate proteoglycans; Syn-4, syndecan-4; CD, cytoplasmic domain; PKCα, protein kinase C-alpha; PtdIns[4,5]P_2, phosphatidylinositol (4,5) bisphosphate; Syn-4ΔV, V domain-lacking syndecan-4; Syn-4ΔC1, C1 domain-lacking syndecan-4; Syn-4ΔC2, C2 domain-lacking syndecan-4; FITC-dex, fluorescently labeled dextran; PDZ, postsynaptic density 95, disc large and zona occludens-1.

* Corresponding authors. Address: Nanoscience and Nanotechnology Research Center, Research Organization for the 21st Century, Osaka Prefecture University, Naka-ku, Sakai, Osaka 599-8570, Japan. Fax: +81 72 254 9895 (I. Nakase). Fax: +81 774 32 3038 (S. Futaki).

E-mail addresses: i-nakase@21c.osakafu-u.ac.jp (I. Nakase), futaki@scl.kyoto-u.ac.jp (S. Futaki).

http://dx.doi.org/10.1016/j.bbrc.2014.03.018
0006-291X/

transduction across cell membranes [10], which act by binding to and activating protein kinase C-alpha (PKCα) [11–13]. *In vitro* experiments have suggested that the multimerization of the core proteins of Syn-4 significantly enhances binding to PKCα; thus, the clustering of Syn-4 that is induced by ligand interactions should control signal transduction [14,15]. The importance of HSPGs for cellular uptake of arginine-rich CPPs has been previously shown [1,2,8,9,16]. The contribution of Syn-4 and potential involvement of PKCα in the cellular uptake of representative arginine-rich CPPs, HIV-1 TAT (48–60) and octaarginine (R8), has been suggested from a study that employed Syn-4 overexpressing cells and inhibitors of a macropinocytosis and PKCα [16]. However, the details of the molecular interplays involved in this activation step of R8 cellular uptake remain unclear.

In the present study, we shed light on the molecular interplays that accompany the initiation of cellular uptake, especially during macropinocytic uptake of R8 on the membrane. We found that the Syn-4 cytoplasmic V domain makes a significant contribution to the cellular uptake of the R8 peptide. Our results indicate that the clustering of Syn-4 on plasma membranes after they interact with R8 and the eventual binding of PKCα to the Syn-4 cytoplasmic V domain should lead to the cellular uptake of arginine-rich CPPs, which encompasses macropinocytic uptake. Furthermore, we found that the C1 and C2 CDs of Syn-4 are not involved in the cellular uptake of R8 peptide.

2. Materials and methods

2.1. Cell culture

Human cervical cancer-derived HeLa cells were purchased from Riken BRC Cell Bank (Ibaraki, Japan) and cultured in α-minimal essential medium containing 10% heat-inactivated bovine serum (α-MEM(+)) (Invitrogen, Eugene, OR). The cells were grown on 100 mm dishes and incubated at 37 °C under 5% CO_2.

2.2. Confocal microscopy

HeLa cells (in glass-bottom dishes) overexpressing Syn-4 and V domain-lacking Syn-4 (Syn-4ΔV) were washed with α-MEM(−) and treated with Alexa488-labeled peptides in α-MEM(−) (200 μL) for 30 min at 37 °C under 5% CO_2. After washing the cells with 0.5 mg/mL heparin in phosphate-buffered saline (PBS), confocal microscopy was conducted using a FV300 confocal scanning laser microscope (Olympus, Tokyo, Japan) equipped with a ×60 objective without fixing the cells.

In the case of examinations for the clustering of Syn-4 derivatives by peptides, the cells (in glass-bottom dishes) were washed with α-MEM(−) (Fig. 2A and B) and incubated with the medium for 15 min at 4 °C before peptide treatment (Fig. 2A). Next, the cells were treated with non-fluorescently labeled peptides in α-MEM(−) (200 μL) for 30 min at 4 °C (Fig. 2A) or for 15 min at 37 °C (Fig. 2B). The cells were fixed with 4% paraformaldehyde (200 μL) for 30 min at 4 °C, then treated with 0.01% Triton X-100 in PBS (200 μL) for 5 min at room temperature. After blocking the cells with 2% fetal bovine serum in PBS (200 μL) for 1 h at 4 °C, the cells were treated with anti-syndecan-4 (5G9; Santa Cruz Biotechnology, Santa Cruz, CA) (5 μg/mL, 200 μL), anti-HA (3F10; Roche Diagnostics, Indianapolis, IN) (5 μg/mL, 200 μL), or anti-PKCα (Enzo Life Sciences, Farmingdale, NY) (4 μg/mL, 200 μL) (30 min, room temperature), followed by treatment with Alexa Fluor 488 goat anti-mouse IgG or Alexa Fluor 568 goat anti-rat IgG (Invitrogen; each 4 μg/mL, 200 μL) (30 min, room temperature). After washing the cells with PBS, confocal microscopy was conducted.

2.3. Flow cytometry

HeLa cells (in 24-well microplates) overexpressing Syn-4, C1 domain-lacking Syn-4 (Syn-4ΔC1), Syn-4ΔV, or C2 domain-lacking Syn-4 (Syn-4ΔC2) were washed with α-MEM(−), and the cells were treated with Alexa488-labeled peptides in α-MEM(−) (200 μL) for 30 min at 37 °C under 5% CO_2 prior to washing with 0.5 mg/mL heparin in PBS. The cells were then treated with 0.01% trypsin at 37 °C for 10 min prior to the addition of PBS (200 μL) and centrifuged at 3000 rpm (800g) for 3 min at 4 °C. After the supernatant was removed, the cells were washed with PBS (400 μL) and centrifuged at 3000 rpm for 3 min at 4 °C. After this washing cycle was repeated, the cells were suspended in PBS (400 μL) and subjected to fluorescence analysis on a FACSCalibur (BD Biosciences, Franklin Lakes, NJ) flow cytometer using 488-nm laser excitation and a 515- to 545-nm emission filter.

2.4. Western blot analysis

HeLa cells overexpressing Syn-4, Syn-4ΔC1, Syn-4ΔV, or Syn-4ΔC2 (6-well microplates) were washed with α-MEM(−) and the cells were treated with peptides in α-MEM(−) (500 μL) for 30 min at 37 °C under 5% CO_2. After peptide treatment, the cells were scraped into lysis buffer (200 μL) (1% octylphenyl-polyethylene glycol, 1% digitonin, and 0.5% Triton X-100) supplemented with protease inhibitor cocktail reagent (Complete, EDTA-free; Roche Diagnostics GmbH, Mannheim, Germany) as described in the manufacturer's protocol. Syn-4 immunoprecipitation was then conducted using Dynabeads Protein G (Invitrogen) bound to anti-Syn-4 antibodies, as described in the manufacturer's protocols. The boiled antigen samples were separated by 8% sodium dodecyl sulfate–polyacrylamide gel electrophoresis, then transferred to polyvinylidene fluoride membranes (GE Healthcare, Waukesha, WI) and treated with anti-PKCα (Enzo Life Sciences). Secondary antibodies labeled with horseradish peroxidase (anti-mouse IgG HRP-linked whole antibody donkey; GE Healthcare) were then used, and immunoreactive species were detected using the ECL Plus Western Blotting Detection System (GE Healthcare).

3. Results and discussion

3.1. Effect of Syn-4 expression on the cellular uptake of R8

R8 is a representative CPP [1,2,8] that has been employed in the delivery of bioactive molecules into various types of cells. We validated the importance of Syn-4 in the cellular uptake of R8 by overexpressing Syn-4 in HeLa cells transfected with a Syn-4 expression vector (Syn-4-HeLa). The cellular uptake of fluorescently labeled R8 (R8-Alexa488) peptides by Syn-4-HeLa was compared to wild-type (WT) non-transfected HeLa cells (Fig. 1A and B). Cells were treated with 5 μM R8-Alexa488 for 30 min at 37 °C (Fig. 1A and B). Punctuated endosome-like signals from R8-Alexa488 peptides were observed in both Syn-4-HeLa and WT cells (Fig. 1A). However, Syn-4-HeLa cells displayed a more intense signal than WT cells treated with R8-Alexa488 peptides. Fluorescence-activated cell sorting (FACS) analysis also indicated a two-fold increase in peptide internalization by Syn-4-HeLa cells (Fig. 1B).

3.2. Syn-4-dependent induction of macropinocytosis by R8

Macropinocytosis has been shown to be one of the major pathways for the cellular uptake of R8 [6–8]. We examined the contribution of Syn-4 to the induction of macropinocytic cellular uptake of R8 (Fig. 1C). When wildtype HeLa cells were treated with Fluorescein isothiocyanate-dextran (FITC-dex, 70 kDa), a marker of

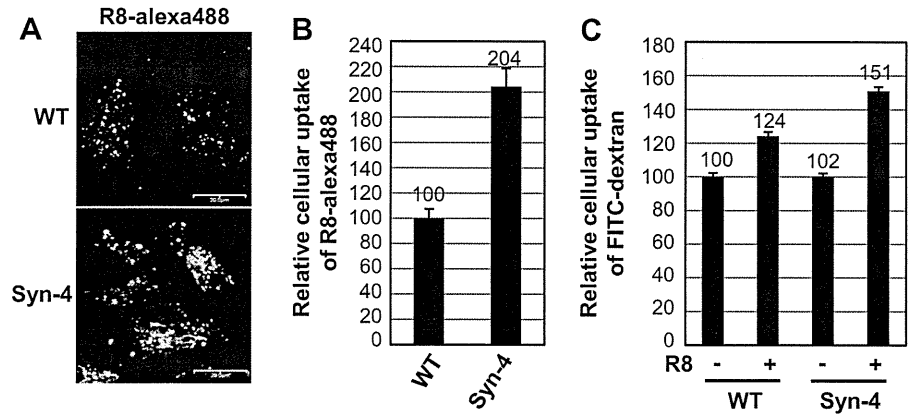

Fig. 1. Syn-4 expression significantly increases the cellular uptake of R8 and FITC-dextran. (A and B) Wildtype (WT)- or Syn-4-overexpressing (Syn-4) HeLa cells were treated with R8-Alexa488 (5 μM) for 30 min at 37 °C, prior to confocal microscopy (A) and FACS analysis (B). Scale bars, 20 μm. The data represent the averages (±SD) of three experiments. (C) WT- or Syn-4 HeLa cells were treated with R8 (5 μM) for 15 min at 37 °C, and were then incubated with FITC-dex (2 mg/mL) for 30 min at 37 °C prior to FACS analysis. The data represent the averages (±SD) of five experiments.

macropinocytosis, R8 (5 μM) enhanced the internalization of FITC-dex by 24% when compared to the case where R8 was not added (Fig. 1C). Conversely, in Syn-4-HeLa cells, R8 strongly stimulated the cellular uptake of FITC-dex (51% higher than that measured in wildtype HeLa cells; Fig. 1C). These results suggest that Syn-4 significantly contributes to the R8-mediated induction of macropinocytosis.

3.3. Induction of Syn-4 clustering on plasma membranes by R8

The effects of R8 on Syn-4 clustering at the plasma membrane are presented in Fig. 2A. Syn-4-HeLa cells were treated with non-fluorescently labeled R8 (10 μM) for 30 min at 4 °C, and immunostaining for Syn-4 was conducted to visualize their locations at the plasma membrane using anti-hemagglutinin epitope (HA) antibodies to detect the HA-tag sequence fused to Syn-4 (Fig. 3A). Under this experimental condition, a low temperature treatment (4 °C) effectively prevented the internalization of membrane molecules by endocytosis. In the presence of R8, comparatively larger-sized fluorescence signals from Syn-4 on the plasma membrane were observed when compared with non-peptide-treated cells (Fig. 2A, Supplementary Fig. S1A). This observation suggests that R8 enhances Syn-4 clustering on plasma membranes during this short period of 30 min. R8-Alexa488 and Syn-4 co-localization was also observed at the plasma membrane (Supplementary Fig. S1B). Conversely, tetraarginine (R4), which has a significantly lower internalization efficiency into cells than R8 [6–17], was largely unable to induce Syn-4 clustering on plasma membranes (Supplementary Fig. S1A). Likewise, Syn-4 did not enhance the cellular uptake of R4 (Supplementary Fig. S2). The observations from our co-localization experiments suggest a strong correlation between Syn-4 clustering and the cellular uptake of arginine-rich CPPs.

3.4. R8 enhances the binding of PKCα to Syn-4 in the cytosol

Next, we examined the effects of R8 on the localization of PKCα inside cells (Fig. 2B). As described in Section 1, PKCα binding to Syn-4 has previously been found to activate PKCα, leading to signal transduction [15]. However, the details regarding the correlations between the extent of Syn-4 clustering, binding of PKCα, and its activation remained unclear. In the present study, Syn-4-HeLa cells were treated with or without R8 (10 μM) for 15 min at 37 °C, and immunostaining for Syn-4 and PKCα was conducted prior to confocal microscopy. Treatment with R8 significantly induced Syn-4 clustering on the plasma membrane, as observed in Fig. 2A, and obvious co-localization of Syn-4 clustering and PKCα

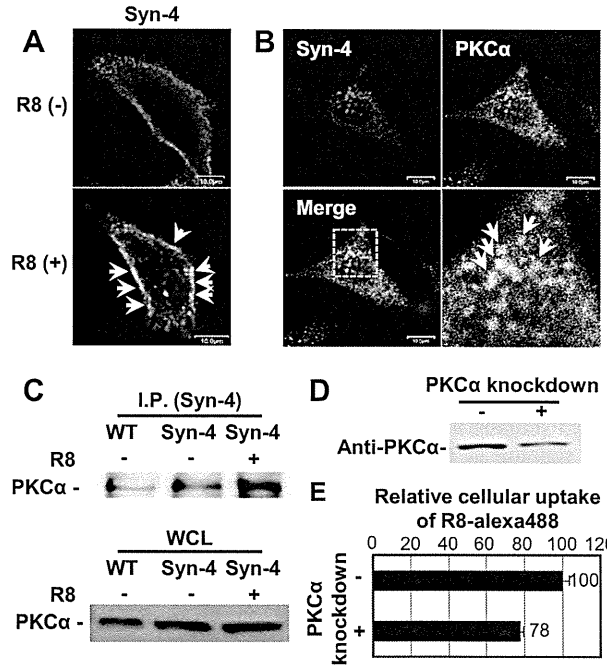

Fig. 2. R8 induces the clustering of Syn-4 on plasma membranes, leading to enhanced binding of PKCα to Syn-4 inside cells. (A) Syn-4-HeLa cells were treated with or without R8 (10 μM) for 30 min at 4 °C prior to immunostaining for Syn-4 (green) and confocal microscopy. Arrows show representative induced clustering of Syn-4. (B) Syn-4-HeLa cells were treated with R8 (10 μM) for 15 min at 37 °C, and immunostaining for Syn-4 (red) and PKCα (green) was conducted prior to confocal microscopy. Arrows show representative co-localization of Syn-4 and PKCα. Scale bar, 10 μm. (C) PKCα binding to Syn-4 was analyzed by Western blotting as described in Section 2. Wildtype (WT) or Syn-4-HeLa cells were treated with R8 (10 μM) for 30 min at 37 °C, then immunoprecipitation (IP) for Syn-4 was conducted from whole-cell lysates (WCL). (D and E) The knockdown of PKCα decreases cellular uptake of R8. (D) The expression level of PKCα in wildtype (WT) or PKCα-knockdown HeLa cells as analyzed by Western blotting. (E) PKCα-knockdown HeLa cells were treated with R8-Alexa488 (5 μM) for 30 min at 37 °C prior to FACS analysis. The data represent the averages (±SD) of three experiments. (For interpretation of the references to color in this figure legend, the reader is referred to the web version of this article.)

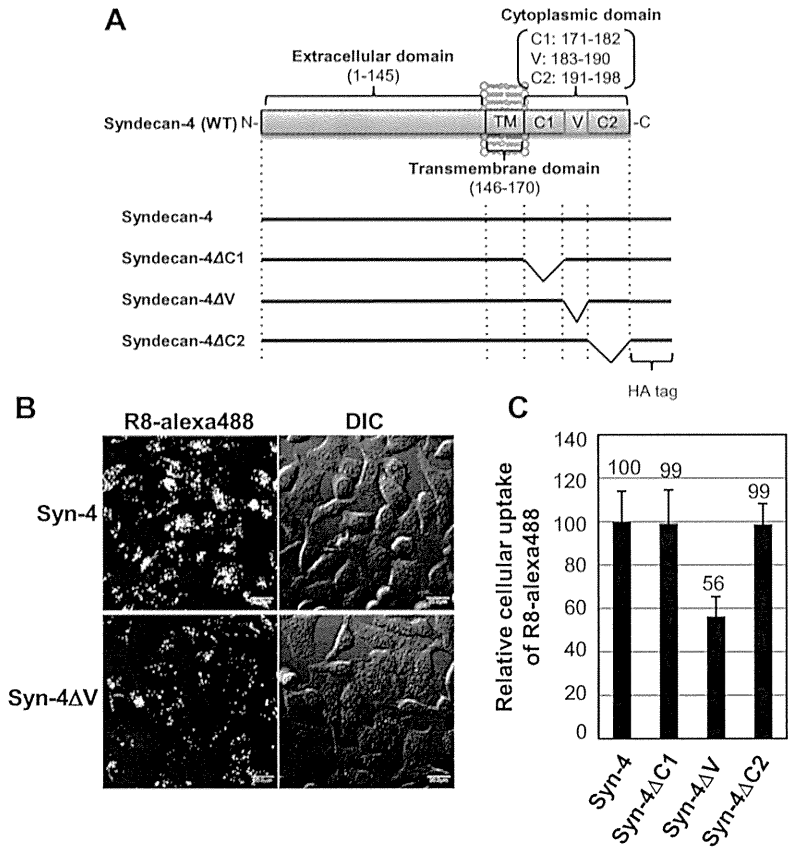

Fig. 3. The V domain of Syn-4 is crucial for the cellular uptake of R8. (A) Schematic representation of Syn-4 derivatives. (B and C) Syn-4- or Syn-4ΔV-HeLa cells were treated with R8-Alexa488 (5 μM) for 30 min at 37 °C prior to confocal microscopy (B). The uptake of R8-Alexa488 (5 μM) in HeLa cells expressing Syn-4 derivatives after 30 min at 37 °C was analyzed by FACS (C). Scale bars, 20 μm. The data represent the averages (±SD) of three experiments.

was also detected (Fig. 2B). In the case of no peptide treatment, uniform staining for Syn-4 at the plasma membrane and diffuse PKCα staining in the cytosol were observed (data not shown). Additionally, in the case of R4, peptide treatment under the same condition did not affect the localization of PKCα inside cells (data not shown). These results suggest that the clustering of Syn-4 by R8 effectively recruits PKCα to Syn-4.

Immunoprecipitation was also conducted using anti-Syn-4 antibodies to detect the interaction between Syn-4 and intracellular molecules as described in Section 2. Western blot analysis showed that the treatment of Syn-4-HeLa cells with R8 (10 μM) for 30 min significantly enhanced the binding of PKCα to Syn-4 (Fig. 2C, upper panel). In whole-cell lysates (WCL), PKCα expression was unaffected by treatment with R8 (Fig. 2C, lower panel), indicating that the expression level of PKCα was not affected during treatment with R8. These results strongly suggest that the induced clustering of Syn-4 after treatment with R8 leads an enhanced intracellular interaction between PKCα and Syn-4.

3.5. PKCα knockdown influences the internalization efficiency of R8 into cells

To confirm the role of PKCα in the cellular uptake of R8, we analyzed the effects of PKCα knockdown by short hairpin RNA (shRNA) treatment on the internalization of the peptide (Fig. 2D and E). In PKCα-knockdown cells, PKCα expression was reduced to about 50% of the levels in non-shRNA-treated cells (Fig. 2D). When the PKCα-knockdown cells were treated with R8-Alexa488 (5 μM) for 30 min at 37 °C, the cellular uptake efficiency of the peptide was decreased by approximately 20% when compared to the control (non-shRNA-treated) cells (Fig. 2E), suggesting that PKCα and its associated signal pathways are involved in the cellular uptake of R8.

3.6. The cytoplasmic V domain of Syn-4 is essential for the cellular uptake of R8

PKCα binds to the V domain of the Syn-4 cytoplasmic region via phosphatidylinositol (4,5) bisphosphate (PtdIns[4,5]P_2) [18,19], which leads to PKCα activation [14,18,20]. To examine how cytosolic PKCα binding to Syn-4 affects the cellular uptake of R8, we constructed a plasmid to express a mutated form of Syn-4 in plasma membranes that lacks the V domain (Syn-4ΔV) (Fig. 3A, Supplementary Fig. S3). Syn-4ΔV-expressing HeLa cells (Syn-4ΔV-HeLa cells) were prepared by transfection of the plasmid as described in the Supplementary materials and methods. We also constructed plasmids to express the C1 domain lacking Syn-4 (Syn-4ΔC1) to prevent the binding of cytoskeletal proteins to Syn-4 inside the cell [21], and to express the C2 domain lacking Syn-4 (Syn-4ΔC2) in plasma membranes to prevent the binding of proteins containing a PDZ domain (postsynaptic density 95, disc large, and zona occludens-1) to Syn-4 (Fig. 3A, Supplementary Fig. S3) [21]. PDZ proteins are known to be important for the induction of Rac1 activation through their binding to Syn-4 (e.g. FGF2) [22,23]. In the present study, Syn-4, Syn-4ΔV, Syn-4ΔC1, and Syn-4ΔC2 expression in HeLa cells was shown to be similar by Western blotting (Supplementary Fig. S3). Immunostaining for heparan sulfate on the plasma membranes of the cells that had

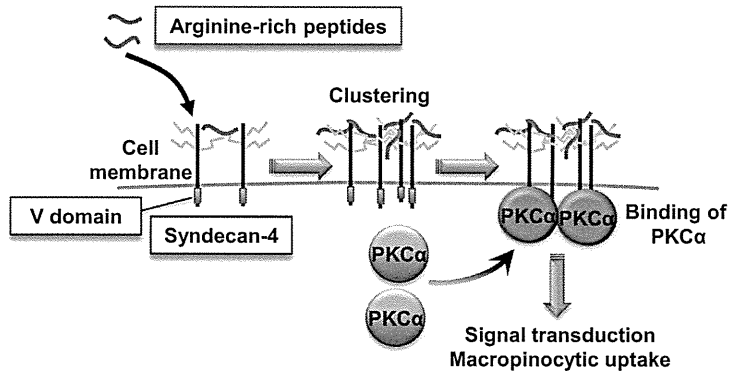

Fig. 4. Schematic diagram of Syn-4 clustering and binding to PKCα inside cells induced by arginine-rich peptides.

been treated with each Syn-4-mutant-expressing plasmid showed similar expression levels (data not shown).

Each mutated Syn-4-expressing HeLa cell line was treated with R8-Alexa488 (5 μM) for 30 min at 37 °C, and the cellular uptake efficiency of the peptide was analyzed using confocal microscopy and FACS (Fig. 3B and C). Deletion of the V domain significantly reduced cellular uptake of the peptide by 44% (Syn-4ΔV-HeLa cells) when compared with Syn-4-HeLa cells (Fig. 3B and C), although R8 enhanced clustering of Syn-4ΔV on the plasma membrane (Supplementary Fig. S4). This suggests a significant contribution of the V domain of Syn-4 to the cellular uptake of R8. Conversely, deletion of C1 (Syn-4ΔC1-HeLa cells) and C2 (Syn-4ΔC2-HeLa cells) domains did not affect the cellular uptake of R8 (Fig. 3C). Moreover, the internalization efficiency of R8-Alexa488 (20 μM), which was expected to enhance cytosolic release of the peptide, was also reduced in Syn-4ΔV-HeLa cells (24%) as determined by FACS (Supplementary Fig. S5B). Confocal microscopic images showed that the signal intensity of R8-Alexa488 that diffusely localized in the cytosol and the nucleus was significantly diminished (Supplementary Fig. S5A). Conversely, the internalization efficiency of the peptide into Syn-4ΔC1- and Syn-4ΔC2-HeLa cells under this experimental condition was similar to that in Syn-4-HeLa cells (Supplementary Fig. S5B). These results suggest that the V domain of Syn-4 is important for the cellular uptake and membrane penetration of R8, and the binding of PKCα to the V domain of Syn-4 is considered to be important as a first cellular event that prompts cellular uptake of the peptide. Additionally, an increase in FITC-dex uptake by Syn-4ΔV-HeLa cells was only 9% of that demonstrated by Syn-4-HeLa cells when treated with R8 (data not shown), suggesting that the induction of macropinocytosis by R8 through the binding of PKCα and Syn-4 is important for cellular uptake of the peptide.

To summarize, our results elucidate the molecular interplays that take place on plasma membranes and contribute to R8 cellular uptake. Specifically, we found that the R8-mediated clustering of Syn-4 leads to PKCα activation, and that the V domain in Syn-4 is critical for this activation (Fig. 4). Although further studies are necessary to obtain more detailed information on the cytoplasmic events following PKCα activation, these findings should have an impact on our understanding of the biological significance of membrane-associated proteoglycans as well as the internalization methods of other macromolecules and viruses.

Conflict of interest

The authors have no conflict of interest to declare.

Acknowledgments

This work was supported in part by Grants-in-Aid for Scientific Research from the Ministry of Education, Culture, Sports, Science and Technology of Japan and Takeda Science Foundation. This work was also supported by the Collaborative Research Program of Institute for Chemical Research, Kyoto University.

Appendix A. Supplementary data

Supplementary data associated with this article can be found, in the online version, at http://dx.doi.org/10.1016/j.bbrc.2014.03.018.

References

[1] S. Futaki, Special theme issue on membrane permeable peptide vectors: chemistry and functional design for the therapeutic applications, Adv. Drug Deliv. Rev. 60 (2008) 447–614.
[2] I. Nakase, H. Akita, K. Kogure, et al., Efficient intracellular delivery of nucleic acid pharmaceuticals using cell-penetrating peptides, Acc. Chem. Res. 45 (2012) 1132–1139.
[3] J.A. Swanson, C. Watts, Macropinocytosis, Trends Cell Biol. 5 (1995) 424–428.
[4] J.A. Swanson, Shaping cups into phagosomes and macropinosomes, Nat. Rev. Mol. Cell Biol. 9 (2008) 639–649.
[5] J.S. Wadia, R.V. Stan, S.F. Dowdy, Transducible TAT-HA fusogenic peptide enhances escape of TAT-fusion proteins after lipid raft macropinocytosis, Nat. Med. 10 (2004) 310–315.
[6] I. Nakase, M. Niwa, T. Takeuchi, et al., Cellular uptake of arginine-rich peptides: roles for macropinocytosis and actin rearrangement, Mol. Ther. 10 (2004) 1011–1022.
[7] I.M. Kaplan, J.S. Wadia, S.F. Dowdy, Cationic TAT peptide transduction domain enters cells by macropinocytosis, J. Control. Release 102 (2005) 247–253.
[8] I. Nakase, A. Tadokoro, N. Kawabata, et al., Interaction of arginine-rich peptides with membrane-associated proteoglycans is crucial for induction of actin organization and macropinocytosis, Biochemistry 46 (2007) 492–501.
[9] I. Nakase, H. Hirose, G. Tanaka, et al., Cell-surface accumulation of flock house virus-derived peptide leads to efficient internalization via macropinocytosis, Mol. Ther. 17 (2009) 1868–1876.
[10] K. Lambaerts, S.A. Wilcox-Adelman, P. Zimmermann, The signaling mechanisms of syndecan heparan sulfate proteoglycans, Curr. Opin. Cell Biol. 21 (2009) 662–669.
[11] E. Okina, T. Manon-Jensen, J.R. Whiteford, J.R. Couchman, Syndecan proteoglycan contributions to cytoskeletal organization and contractility, Scand. J. Med. Sci. Sports 19 (2009) 479–489.
[12] J.R. Couchman, Syndecans: proteoglycan regulators of cell-surface microdomains?, Nat Rev. Mol. Cell Biol. 4 (2003) 926–937.
[13] M. Simons, A. Horowitz, Syndecan-4-mediated signaling, Cell. Signal. 13 (2001) 855–862.
[14] E.S. Oh, A. Woods, J.R. Couchman, Multimerization of the cytoplasmic domain of syndecan-4 is required for its ability to activate protein kinase C, J. Biol. Chem. 272 (1997) 11805–11811.
[15] E.S. Oh, A. Woods, J.R. Couchman, Syndecan-4 proteoglycan regulates the distribution and activity of protein kinase C, J. Biol. Chem. 272 (1997) 8133–8136.
[16] T. Letoha, A. Keller-Pintér, E. Kusz, et al., Cell-penetrating peptide exploited syndecans, Biochim. Biophys. Acta 1798 (2010) 2258–2265.

[17] M. Kosuge, T. Takeuchi, I. Nakase, et al., Cellular internalization and distribution of arginine-rich peptides as a function of extracellular peptide concentration, serum, and plasma membrane associated proteoglycans, Bioconjug. Chem. 19 (2008) 656–664.
[18] E.S. Oh, A. Woods, S.T. Lim, et al., Syndecan-4 proteoglycan cytoplasmic domain and phosphatidylinositol 4,5-bisphosphate coordinately regulate protein kinase C activity, J. Biol. Chem. 273 (1998) 10624–10629.
[19] D. Lee, E.S. Oh, A. Woods, et al., Solution structure of a syndecan-4 cytoplasmic domain and its interaction with phosphatidylinositol 4,5-bisphosphate, J. Biol. Chem. 273 (1998) 13022–13029.
[20] A. Horowitz, M. Murakami, Y. Gao, M. Simons, Phosphatidylinositol-4,5-bisphosphate mediates the interaction of syndecan-4 with protein kinase C, Biochemistry 38 (1999) 15871–15877.
[21] E. Tkachenko, J.M. Rhodes, M. Simons, Syndecans: new kids on the signaling block, Circ. Res. 96 (2005) 488–500.
[22] Y. Gao, M. Li, W. Chen, M. Simons, Synectin, syndecan-4 cytoplasmic domain binding PDZ protein, inhibits cell migration, J. Cell. Physiol. 184 (2000) 373–379.
[23] E. Tkachenko, A. Elfenbein, D. Tirziu, M. Simons, Syndecan-4 clustering induces cell migration in a PDZ-dependent manner, Circ. Res. 98 (2006) 1398–1404.

1. Fallon SC, Brandt ML, Rodriguez JR, *et al.* Cytogenetic analysis in the diagnosis and management of lipoblastomas: results from a single institution. *J Surg Res* 2013; 184: 341-6.
2. Chung EB, Enzinger FM. Benign lipoblastomatosis. An analysis of 35 cases. *Cancer* 1973; 32: 482-92.
3. Dutton JJ, Escaravage GK Jr., Fowler AM, Wright JD. Lipoblastomatosis: case report and review of the literature. *Ophthal Plast Reconstr Surg* 2011; 27: 417-21.
4. Speer AL, Schofield DE, Wang KS, *et al.* Contemporary management of lipoblastoma. *J Pediatr Surg* 2008; 43: 1295-300.
5. Kamal NM, Jouini R, Yahya S, Haiba M. Benign intrascrotal lipoblastoma in a 4-month-old infant: a case report and review of literature. *J Pediatr Surg* 2011; 46: E9-12.
6. Mognato G, Cecchetto G, Carli M, Talenti E, d'Amore ES, Pederzini F, Guglielmi M. Is surgical treatment of lipoblastoma always necessary? *J Pediatr Surg* 2000; 35: 1511-3.
doi:10.1684/ejd.2014.2333

Pseudoxanthoma elasticum-like skin lesions with congenital erythropoietic porphyria

Pseudoxanthoma elasticum (PXE) is a rare autosomal recessive disorder characterized by ectopic mineralization of connective tissue in the skin, eyes and vascular organs. Multiple small yellowish papules appear in the skin in the flexion areas of large joints, the neck and the periumbirical region. Calcified degenerated elastic fibers are observed upon pathological analysis. PXE is caused by mutations in the *ABCC6* gene; however, it is not known how such mutations contribute to the symptoms of PXE [1]. Congenital erythropoietic porphyria (CEP) is caused by the almost complete absence of the enzyme uroporphyrinogen III synthase (UROIIIS), which participates in the production of heme. This results in the accumulation of porphyrins and a reduction in red blood cell production [2]. CEP causes severe cutaneous sensitivity to visible light and often requires blood transfusions to treat anemia. Histopathological characteristics are scarring and subepidermal blistering because of photosensitivity, but no elastic fiber degeneration. To our knowledge, there are no reports of PXE-like skin lesions in the setting of porphyria. Here, we present the first case of a patient with PXE-like lesions and CEP.

A 41-year-old Japanese woman presented with multiple skin lesions on her neck and the anterior surfaces of her arms. She was diagnosed with CEP shortly after birth and harbored the nonsense mutation Q249X in UROIIIS [3]. For about 40 years, she had received blood transfusions for severe anemia and multiple skin graft operations on her face and hands to treat refractory skin ulcers, (*figures 1A-B*) but she had not undergone liver transplantation. A physical examination revealed sclerodermoid changes, exclusively restricted to the light-exposed areas, and normal skin in the light-unexposed areas, such as the trunk, medial side of forearms, etc. On the cheeks, nose, and the neck, there were yellowish papules (*figures 1A-C*). There were small grayish papules with black dots concomitant with confluent yellowish papules on the anterior and lateral aspects of her neck (*figure 1C*) and on the lateral side of her forearms (*figures 1D-E*), which have not been described in patients with PXE. All her fingers were sclerotic and some were shortened due to repeated unhealed skin ulcers (*figure 1B*). Histopathological examination of the lesion on her forearm revealed a large, calcified mass and basophilic wavy fibers in the mid-dermis (*figures 1F-G*). Elastica van Gieson staining revealed degenerated and fractured elastic fibers (*figure 1H*) and von Kossa staining showed that the degenerated elastic fibers were calcified (*figure 1I*). The calcium deposition of elastic fibers in the present case is not known in solar elastosis due to photodamage or in dystrophic calcification secondary to photosensitivity of the porphyria cutanea tarda patient [4]. Berlin blue staining did not detect iron deposition. Ophthalmologic examination identified angioid streaks and subretinal hemorrhages in both eyes. Direct sequence of all 31 exons of *ABCC6* after PCR amplification was performed, using specific primers designed with Primer3 software; however, there was no pathological mutation.

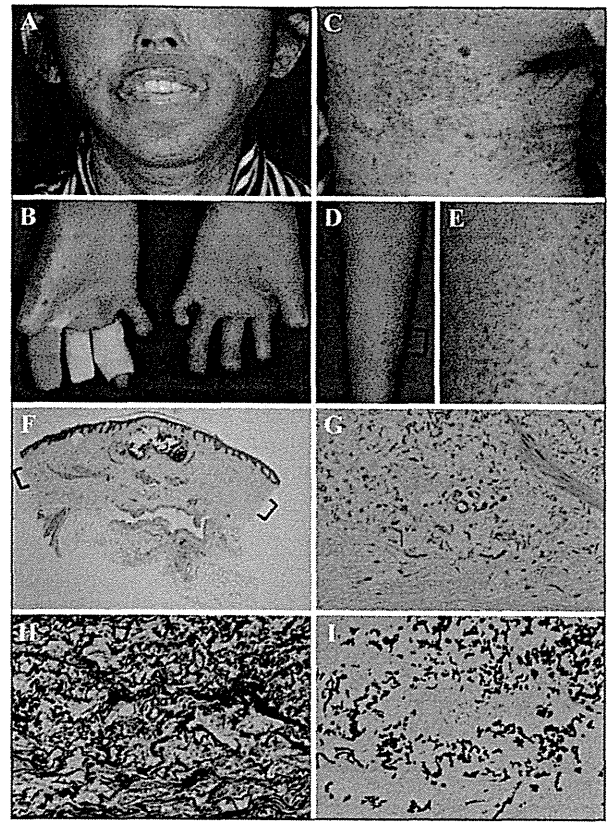

Figure 1. A) Yellowish papules on the sclerotic cheeks, nose and neck. Skin graft covered perioral area. **B)** Sclerodermoid changes on the palms and fingers. Skin ulcers persisted on the shortened right fingers. **C)** Yellowish and grayish papules with black dots were located on her neck **(C)** and on the light-exposed lateral side of the left forearm **(D). E)** Magnified picture of the portion depicted with parenthesis in **(D). F)** Histopathology from the forearm lesion showed a large calcified mass in the center and basophilic materials in the mid-dermis. (Hematoxylin-eosin (HE) stain; original magnification ×40) **G)** Basophilic fibers in a magnified picture of the dermis indicated by parentheses in **(F).** (HE stain) **H)** Distorted and fragmented elastic fibers. (Elastica van Gieson stain) **I)** Calcified elastic fibers. (von Kossa stain) **G-I)** Stain using serial section and original magnification; ×200.

PXE-like symptoms are associated with certain cases of haemoglobinopathy, including β -thalassaemia and sickle-cell disease [5-8]. A systematic study of 100 patients with thalassaemia in Greece showed that 16% had PXE cutaneous lesions and 10% had both PXE lesions and angioid streaks [5]. In another study, 14 of 80 β-thalassaemia patients had PXE-like skin lesions with elastic fiber fragmentation and calcification [6]. In β-thalassaemia, unbound fractions of globin and heme are presumed to result in high levels of oxidative stress, which may cause elastic tissue injury [7]. Furthermore, iron overload by repeated blood transfusions can markedly damage elastic fibers in tissue [8]. On the other hand, a PXE-like phenotype in haemoglobinopathy may be directly provoked by ABCC6 function deficiency, as suggested by a mouse model of thalassaemia that demonstrated ABCC6 transcription decrease [9]. The genes that mutated in PXE and β -thalassaemia might share common metabolic pathways or might be interdependently or independently required for proper maintenance of elastic fibers [10]. In the present patient with porphyria who had extremely severe photosensitivity, distribution of the lesion was strictly limited to light exposed areas, suggesting that photo-induced excitation energy from porphyrin may play a role in the initiation or development of elastic fiber degeneration and calcification, which is not observed in the other haemoglobinopathy or classical PXE. ■

Disclosure. *Financial support: none. Conflict of interest: none.*

[1] Department of Dermatology,
[2] Department of Global Health,
Nagasaki University Graduate School of Biomedical Sciences,
1-7-1 Sakamotomachi, Nagasaki, Japan
<utani@nagasaki-u.ac.jp>

Yoshiko MINE[1]
Akira IWANAGA[1]
Susumu IKEHARA[1]
Yuta KOIKE[1]
Noboru TAKAMURA[2]
Atsushi UTANI[1]

1. Uitto J, Li Q, Jiand Q, *et al.* Pseudoxanthoma elasticum: molecular genetics and putative pathomechanisms. *J Invest Dermatol* 2010; 130: 661-70.
2. Dawe SA, Peters TJ, Du Vivier A, *et al.* Congenital erythropoietic porphyria: dilemmas in present day management. *Clin Exp Dermatol* 2002; 27: 680-3.
3. Tanigawa K, Bensidhoum M, Takamura N, *et al.* A novel point mutation in congenital erythropoietic porphyria in two members of Japanese family. *Hum Genet* 1996; 97: 557-60.
4. Nogueira A, Moreira E, Santos P, Azevedo F. Calcinosis cutis in porphyria cutanea tarda – not always a marker of disease activity. *Eur J Dermatol* 2009; 19: 280-1.
5. Aessopos A, Savvides P, Stamatelos G, *et al.* Pseudoxanthoma elasticum-like skin lesions and angioid streaks in beta-thalassemia. *Am J Hematol* 1992; 41: 159-64.
6. Cianciulli P, Sorrentino F, Maffei L, *et al.* Cardiovascular involvement in thalassaemic patients with pseudoxanthoma elasticum-like skin lesions: a long-term follow-up study. *Eur J Clin Invest* 2002; 32: 700-6.
7. Yu S, Ming A, Wegman A. Pseudoxanthoma elasticum-like lesions in association with thalassaemia major. *Australas J Dermatol* 2009; 50: 186-9.
8. Aessopos A, Samarkos M, Voskaridou E, *et al.* Arterial calcifications in beta-thalassemia. *Angiology* 1998; 49: 137-43.
9. Martin L, Douet V, VanWart CM, Heller MB, Le Saux O. A mouse model of β-thalassemia shows a liver-specific down-regulation of Abcc6 expression. *Am J Pathol* 2011; 178: 774-83.
10. Baccarani-Contri M, Bacchelli B, Boraldi F, *et al.* Characterization of pseudoxanthoma elasticum-like lesions in the skin of patients with β -thalassemia. *J Am Acad Dermatol* 2001; 44: 33-9.

doi:10.1684/ejd.2014.2335

Generalized pustulosis associated with disseminated *Mycobacterium avium* infection in a non-AIDS patient

Non-tuberculous mycobacteria cause opportunistic infectious diseases in immunocompromised patients. Disseminated *Mycobacterium avium* infection occurs frequently in AIDS patients. Here, we describe a case of generalized aseptic pustulosis spread from palmoplantar pustules associated with disseminated *M. avium* infection in a non-AIDS patient.

A 54-year-old Japanese woman visited a local hospital with a several-week history of non-pruritic eruptions. At presentation, there were multiple pustules on the palms and soles, together with arthralgia in bilateral shoulder and knee joints. She was treated with oral prednisolone (20 mg/day) and topical clobetasol propionate for 2 months, which led to improvement of the symptoms. After decreasing the dose of prednisolone, she was treated only with topical clobetasol propionate. The patient's response with regard to the pustules and arthralgia was variable, with improvement seen on some visits but worsening noted on others. One year later, eruptions rapidly spread over the entire body together with fever of 39 °C and exacerbation of arthralgia. She was then referred to our hospital. Examination showed numerous isolated pustules, 2-7 mm in diameter, surrounded by erythema on the trunk and extremities as well as the palms and soles *(figure 1A)*. Subcutaneous lymph nodes were palpable in the right neck region.

Routine laboratory examinations showed an increased white blood cell count of 20,390/mm^3 (neutrophils 84%, lymphocytes 11.7%) and elevated C-reactive protein level of 15.8 mg/dL (normal range, 0-0.10 mg/dL). Liver and renal function tests were normal. Serum IgG was increased (3,710 IU; normal range, 870-1,700 IU). She was negative for anti-nuclear antibody. T cell function was almost normal as follows: CD4/8 ratio, 0.92 (normal range, 0.60-2.90); mitogen-induced blastoid transformation of lymphocytes with PHA, 23,100 (normal range, 20,500-56,800); that with ConA, 19,500 (normal range, 20,300-65,700). Bacterial culture from the pustules yielded no colonies. Skin biopsy from the pustules showed unilocular intraepidermal abscesses with intense neutrophil infiltration *(figure 1B)*. Epidermal spongiosis was not observed.

Computed tomography and magnetic resonance imaging indicated systemic lymph node enlargement as well as scattered nodular shadows in the liver and bilateral lungs and osteolysis in lumbar vertebrae *(figures 1C-E)*. Cervical lymph node biopsy showed granulomatous alteration with microabscess and necrotic materials *(figure 1F)*. The histopathological features suggested the possibility of mycobacterial infection, cat scratch disease, sarcoidosis and others. No mycobacteria were detected from skin or lymph nodes. Warthin-Starry silver stain and PCR for

Cold agglutinin disease-associated digital gangrene treated with plasmapheresis

Sir,

Cold agglutinin disease (CAD) is a type of autoimmune hemolytic anemia. Cold agglutinins are usually immunoglobulin M (IgM) antibodies that bind to erythrocyte surface antigens at low temperatures. Primary cold agglutinin disease is characterized by synthesis of kappa monoclonal IgM antibodies by proliferating clonal B-lymphocytes whereas in secondary disease, synthesis of polyclonal IgM cold agglutinins accompanies acute infections and malignant lymphoma. More than 90% of patients have cutaneous lesions such as reversible acrocyanosis, Raynaud's phenomenon, and livedo reticularis.[1] Since agglutination is rapidly reversible on warming, cold agglutinins rarely cause permanent obstruction of blood vessels leading to digital gangrene.[2-4]

A 54-year-old Japanese man had observed transient digital color changes during each cold season of the past decade. He had no history of underlying diseases, infections, or trauma. In January 2011, his fingers and toes discolored rapidly to gray-black. This was associated with sharp pain which had started 1 week earlier. A physical examination on admission revealed that several fingers and toes were cyanotic and some of the digits had dry gangrene along with marked peripheral coldness [Figure 1a–c]. Routine laboratory investigations indicated moderate hemolytic anemia (hemoglobin level of 8.3 g/dL, unconjugated bilirubin level of 1.3 mg/dL), elevated lactate dehydrogenase (LDH) levels (1,056 IU/L) and increased total IgM levels (456 mg/dL), and revealed a fasting sugar level of 278 mg/dL, then diagnosed as poorly controlled type 2 diabetes (T2DM). A coagulation study including cryoglobulins and cryofibinogen revealed that blood clotting was unaffected. A direct Coombs test showed that C3b and C3d were bound to erythrocyte surface antigens. In addition, cold agglutinin tests revealed elevated titers of 1:1,024 at 4°C and 1:512 at 12°C, while no agglutination was detected at 25°C. Serological studies for viral infections and autoantibodies associated with collagen disease were negative. No malignancy was identified using computed tomography (CT). Monoclonal IgM-kappa protein was detected by immunoelectrophoretic analysis of the patient's serum. Consequently, primary cold agglutinin disease was diagnosed. Bone marrow aspiration showed discrete hyperplasia but no signs of lymphoproliferative disorders. A peripheral blood smear showed clumping of adherent erythrocytes [Figure 1d]. A skin biopsy from a discolored finger revealed thromboembolic changes in capillaries located in the uppermost dermis and endothelial proliferation associated with thrombosis in the subcutaneous tissue [Figure 1e and f].

Although the patient's extremities were kept warm and treated with vasodilating agents, new gangrenous lesions appeared on the fingers. Weekly double-filtration plasmapheresis (DFPP) up to 3,000 ml of plasma per treatment using cascadeflo EC-50W was started to reduce cold agglutinins. After commencing plasmapheresis, total IgM levels rapidly decreased to half or less and cold agglutinin titers at 4°C dropped from 1 in 1024 to 1:128. Further gangrene did not develop and autoimmune

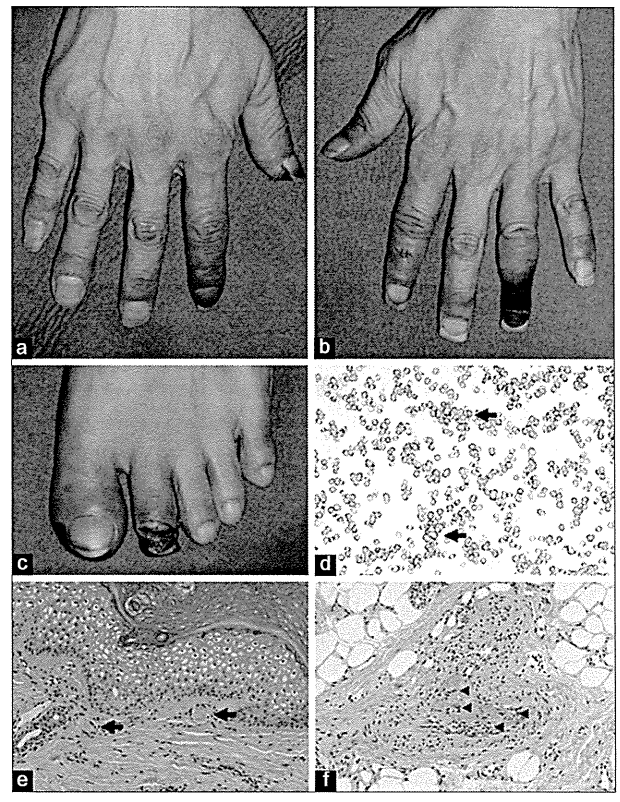

Figure 1: (a-c) Clinical features of the CAD patient. Acrocyanosis and digital gangrene rapidly appeared in the patient's hands and feet. (d) A blood smear test revealed erythrocytic coagulation. The arrow indicates a representative agglutination. Histopathological examination of the cyanotic lesion on the finger revealed thrombosis (arrow) in superficial dermal vessels (e) and endothelial proliferation (arrowhead) associated with thrombosis in subcutaneous vessels (f). (e and f: H and E, ×200)

hemolysis was no longer detected. In all, nine sessions of double-filtration plasmapheresis was undertaken. Finally, debridement and reepithelialization of the gangrenous areas was achieved.

It is known that cold agglutinin disease rarely leads to digital gangrene. However, in the present case it can be postulated that the patient's untreated type 2 diabetes mellitus may have, at least in part, precipitated insufficient circulation due to cold agglutinin disease-induced thromboembolism. Therefore, cold agglutinin disease should be recognized as a risk factor for digital gangrene when it is present in a patient with diabetes. A previous report has suggested that glomeruloid reactive angioendotheliomatosis is a distinct histological feature of the necrotic lesions seen in cold agglutinin disease.[2] This is consistent with the thrombosis-associated endothelial proliferation observed in the subcutaneous tissue of our patient. Treatment for the disease depends on its etiology and severity. Rigorous avoidance of cold exposure is generally considered to be effective treatment for cutaneous lesions.[2,3] Vasodilating agents can also be used to facilitate passage of blood clots through peripheral vessels but were not very effective in our patient. In contrast, antiplatelet agents or anticoagulant drugs were not employed because cold agglutination does not require platelets and clotting factors. In primary cold agglutinin disease, not all patients require pharmacological therapy and immunosuppressive agents such as corticosteroids are almost ineffective.[1] The most efficient therapy is administration of fludarabine and rituximab in combination, although toxicity may be a concern.[5] In the future, double-filtration plasmapheresis which is expected to directly reduce the cold agglutination and to improve clinical symptoms should be studied in greater detail as a treatment for acute exacerbations of cold agglutinin disease with high titers of cold agglutinin.

Yuta Koike, Yuichiro Akiyama, Atsushi Utani

Department of Dermatology, Nagasaki University Graduate School of Biomedical Sciences, Nagasaki, Japan

Address for correspondence: Dr. Atsushi Utani, Department of Dermatology, Nagasaki University Graduate School of Biomedical Sciences, 1-12-4 Sakamoto, Nagasaki 852-8523, Japan.
E-mail: utani@nagasaki-u.ac.jp

REFERENCES

1. Berentsen S, Tjonnfjord GE. Diagnosis and treatment of cold agglutinin mediated autoimmune hemolytic anemia. Blood Rev 2012;26:107-15.
2. Porras-Luque JI, Fernandez-Herrera J, Dauden E, Fraga J, Fernandez-Villalta MJ, Garcia-Diez A. Cutaneous necrosis by cold agglutinins associated with glomeruloid reactive angioendotheliomatosis. Br J Dermatol 1998;139:1068-72.
3. Ciejka JZ, Cook EB, Lawler D, Martin J, Woodson RD, Graziano F. Severe cold agglutinin disease and cryoglobulinemia secondary to a monoclonal anti-Pr2 IgM lambda cryoagglutinin. Clin Exp Rheumatol 1999;17:227-31.
4. Jeskowiak A, Goerge T. Images in clinical medicine. Cutaneous necrosis associated with cold agglutinins. N Engl J Med 2013;369:e1.
5. Berentsen S, Randen U, Vagan AM, Hjorth-Hansen H, Vik A, Dalgaard J, *et al.* High response rate and durable remissions following fludarabine and rituximab combination therapy for chronic cold agglutinin disease. Blood 2010;116:3180-4.

Access this article online	
Quick Response Code:	Website: www.ijdvl.com
	DOI: 10.4103/0378-6323.144221

international wound journal

International Wound Journal ISSN 1742-4801

LETTER TO THE EDITOR

Sacral pressure ulcer successfully treated with traction, resulting in a reduction of wound deformity

Dear Editors,

A pressure ulcer is defined as skin and soft tissue damage caused by external force on a bony prominence (1). Deep pressure ulcers that reach the subcutaneous or underlying tissues are often intractable. It is thought that the undermining formation characteristically observed in pressure ulcers can be attributed to difficulties in treatment. However, the pathogenesis of the undermining formation in pressure ulcers is not yet fully understood. Excision and/or removal of the flap over the undermining area has been reported to be effective for treatment of pressure ulcers, but these procedures are invasive in nature (2). Here, we report the case of a patient with a pressure ulcer who was successfully treated using a traction with bandage. Knowledge about the physical properties of pressure ulcers is critical for understanding this less-invasive treatment procedure.

An 81-year-old Japanese man was referred to our hospital with an enormous pressure ulcer on his sacrum. He could not walk because of disuse syndrome, but was able to seat himself in a chair. Laboratory findings were normal except for a low serum albumin level (2.7 g/dl). At his initial examination, the patient's pressure ulcer severity was D4 E6 s12 i1 g3 n0 P12, and the undermining area was 81 cm^2as determined by the DESIGN-R criteria (3) (Figure 1A). The

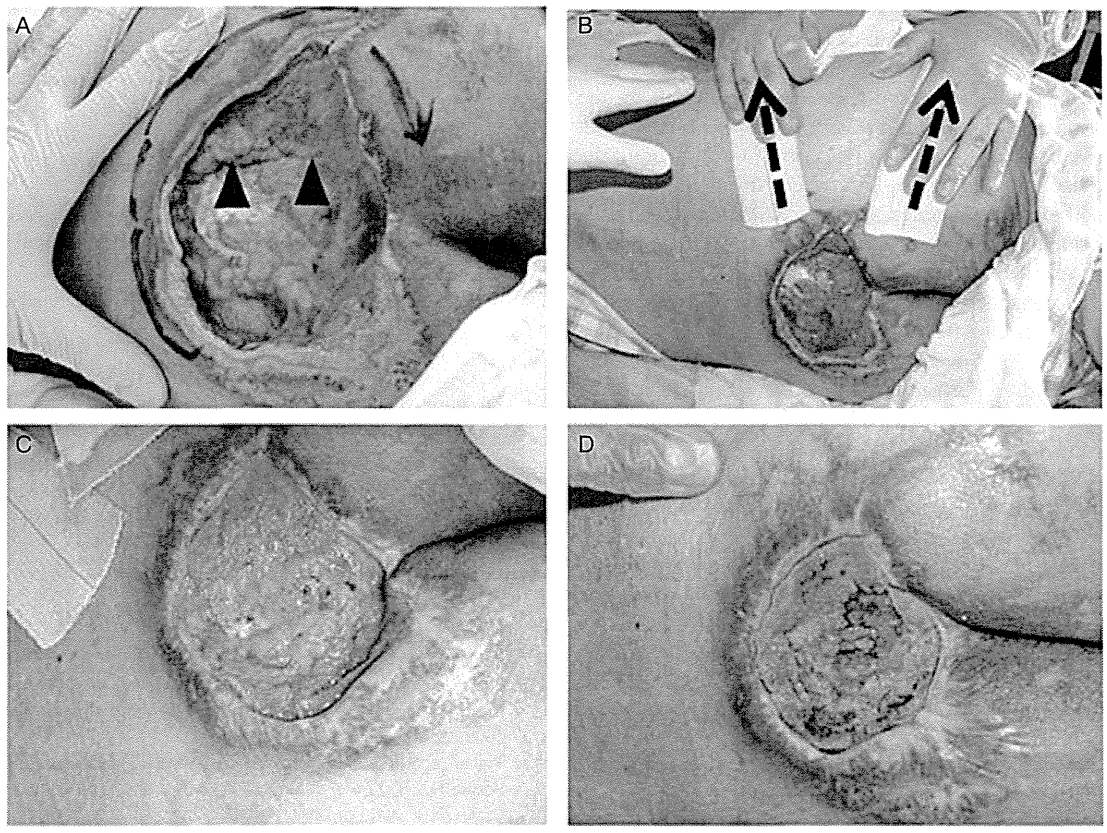

Figure 1 Appearance of stage IV pressure ulcer over the sacrum. (A) Appearance at the initial examination in our hospital is shown. The undermining area of the wound was marked by oiled pen. Granulation tissues appear to be edematous and layered (arrowhead). (B) In order to reduce wound deformity, the wound was treated with traction with elastic bandage towards the right side (broken arrow). (C) Layered granulation tissue disappeared within 1 week. (D) After 5 weeks, wound deformity was no longer observed. Severity of pressure ulcer, as determined by the DESIGN-R criteria, was as follows: (A) D4 E6 s12 i1 G5 n3 P12, (B) D4 E6 s12 i1 g3 n3 P12, (C) D4 e3 s9 i0 g1 n0 p0 and (D) D4 e1 s9 i0 g1 n0 p0.

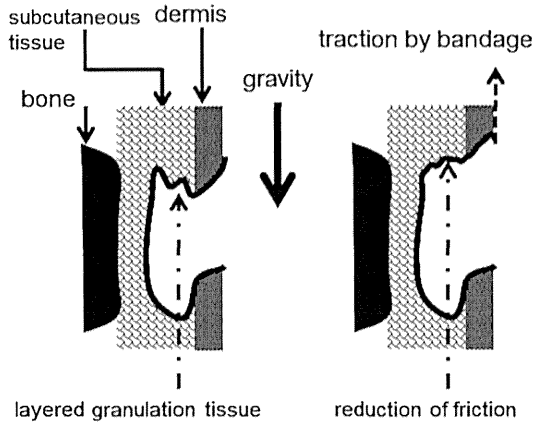

Figure 2 A schematic representation of the physical properties of wounds changed by traction. A cross-sectional model for undermining pressure ulcers onto the sacrum is shown. In the lateral position, external gravitational force is indicated by an arrow, and the direction for traction with bandage is indicated by the broken arrow. Traction with bandage reduces the deformity of the wound and relieves the friction of the wound as shown.

ulcer also exhibited marked wound deformity. Granulation tissues in the wound appeared to be edematous, with a layered appearance, particularly at the edge of the wound (Figure 1A). The layered granulation tissue seemed to be caused by the deformity of the wound. The pressure ulcer was treated with an iodine-containing ointment (U-pasta^{TM}) throughout the initial observation period. After 1 week, in order to reduce the wound deformity, traction with elastic bandage was used after informed consent was obtained (Figure 1B). Traction force was applied in the direction indicated by the broken arrows. The conceptual diagram for the traction treatment is shown in Figure 2. After wound traction with the bandage was performed for 5 weeks, the patient's wound deformity reduced markedly. Furthermore, the traction alleviated the pressure ulcer, as showed by the improved DESIGN-R score. Notably, the layered granulation tissue disappeared within 1 week (Figure 1C). Five weeks after the treatment, traction with bandage was discontinued due to a marked reduction of the patient's wound deformity (Figure 1D).

The pathogenesis of undermining formation in pressure ulcers is not fully understood. Ohura *et al.* (4) concluded that undermining formation in pressure ulcers is caused by the discharge of liquefied necrosis and/or external forces. However, complete elimination of external force on the wound is usually difficult because of the limited movement capability of patients. Particularly, the force of gravity onto the pressure ulcer could not be reduced even if the wound was not directly pressed. Therefore, a simple and non-invasive method using traction with a bandage could be beneficial for minimising the wound deformity. Theoretically, traction does not reduce the external force onto the pressure ulcer. However, it can alleviate wound deformity, which makes the potential benefit of this procedure noteworthy and meriting of further research. Therefore, understanding the concept of reduced wound deformity may be important for this procedure (Mizokami *et al.*, accompanying manuscript). Consequently, we suggest that the physical properties of the wound should be given careful consideration during treatment and care of pressure ulcers with undermining formation, especially on the sacrum.

Acknowledgements

Funding for this study was provided by Research Funding for Longevity Sciences (21A-18) (to ZI, KF and AU) from the National Center for Geriatrics and Gerontology (NCGG), Japan. The authors have no conflicts of interest.

Fumihiro Mizokami, BS
Department of Pharmacy
National Center for Geriatrics and Gerontology
Obu, Aichi, Japan

Katsunori Furuta, BS
Departments of Pharmacy, and Clinical Research and Development
National Center for Geriatrics and Gerontology
Obu, Aichi, Japan

Hisako Matsumoto, RN, PhD
Department of Fundamental Nursing
Mie Prefectural College of Nursing, Tsu, Mie, Japan

Atsushi Utani, MD, PhD
Department of Dermatology
Graduate School of Biomedical Sciences
Nagasaki University
Nagasaki, Japan

Zenzo Isogai, MD, PhD
Department of Advanced Medicine
Division of Dermatology and Connective Tissue Medicine
National Center for Geriatrics and Gerontology
Obu, Aichi, Japan
zenzo@ncgg.go.jp
doi: 10.1111/j.1742-481X.2012.01028.x

References

1. Shea JD. Pressure sores: classification and management. *Clin Orthop Relat Res* 1975;**112**:89–100.
2. Schiffman J, Golinko MS, Yan A, Flattau A, Tomic-Canic M, Brem H. Operative debridement of pressure ulcers. *World J Surg* 2009;**33**:1396–402.
3. Matsui Y, Furue M, Sanada H, Tachibana T, Nakayama T, Sugama J, Furuta K, Tachi M, Tokunaga K, Miyachi Y. Development of the DESIGN-R with an observational study: an absolute evaluation tool for monitoring pressure ulcer wound healing. *Wound Repair Regen* 2011;**19**:309–15.
4. Ohura T, Ohura N. Pathogenetic mechanisms and classification of undermining in pressure ulcers – elucidation of relationship with deep tissue injuries. *Wounds* 2006;**18**:329–39.

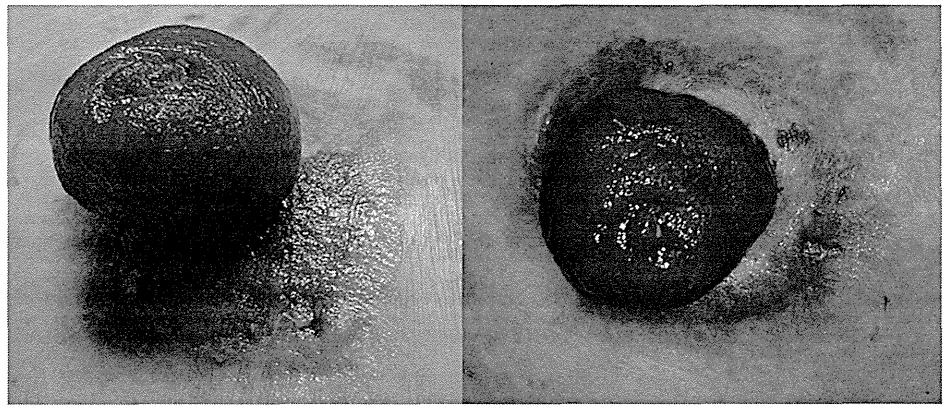

Fig 2. Ileostomy with cutaneous intestinal metaplasia. Before treatment (punch biopsy site at 4 o'clock; *left*). After treatment (*right*).

of EMA, CAM5.2 and CK20. Ki-67 proliferative index was not increased. Overall, these findings suggested a metaplastic phenomenon.

Our patient returned to clinic for suture removal (Fig 2, left) and at that time was treated with electrocoagulation on a focal 1-cm region of the erosion. On follow-up visit, the treated erosion had evidence of reepithelialization and additional areas of the erosion were treated, with a total of 4 sessions of electrocoagulation scheduled 4 weeks apart (Fig 2, right). Repeat punch biopsy performed at the conclusion of therapy was consistent with cicatrix, without evidence of intestinal metaplasia.

Peristomal intestinal metaplasia has been rarely described.[1-4] We report a second case of intestinal metaplasia in a flat peristomal ulcer without overgranulation, with an emphasis on management of this condition. The pathogenesis is hypothesized to be related to dissemination of intestinal mucosal cells into the peristomal skin during surgery, or the promotion of colonic mucosa migration and growth by bile salts in intestinal contents.[5]

In 1 previous case report of peristomal intestinal metaplasia, the authors induced effective reepithelialization of the erosion after 11 electrocoagulation treatments,[2] based on the hypothesis that destruction of intestinal tubular glands eliminates the secreted factors that may promote the erosion. Given reports of primary adenocarcinoma at sites of intestinal metaplasia,[4] when evaluating a patient with a peristomal erosion recalcitrant to therapy, it is recommended that a biopsy be performed to establish the nature of the peristomal skin changes and to guide proper treatment and management.

Kseniya Golubets, MD,[a] Oana M. Radu, MD,[b] Jonhan Ho, MD,[b] and Lisa M. Grandinetti, MD, FAAD[a]

Department of Dermatology[a] and Department of Dermatopathology,[b] University of Pittsburgh Medical Center, Pittsburgh, Pennsylvania

Funding sources: None.

Conflict of interest: None declared.

Correspondence to: Lisa M. Grandinetti, MD, FAAD, University of Pittsburgh, Department of Dermatology, Presbyterian South Tower, Suite 3880, 200 Lothrop Street, Pittsburgh, PA 15213

E-mail: grandinettilm@upmc.edu

REFERENCES

1. Lyon CC, Smith AJ, Griffiths CE, Beck MH. The spectrum of skin disorders in abdominal stoma patients. Br J Dermatol 2000; 143:1248-60.
2. Ono R, Oka M, Sakaguchi M, Kawakami F, Nagano T, Kunisada M, et al. Peristomal skin ulcer with intestinal metaplasia. Br J Dermatol 2012;167:204-6.
3. Johnson CD, White H. Colonic metaplasia with colonic-type polyps on an ileostomy stoma in polyposis coli. Report of a case. Dis Colon Rectum 1988;31:405-7.
4. Berman JJ, Ullah A. Colonic metaplasia of ileostomies. Biological significance for ulcerative colitis patients following total colectomy. Am J Surg Pathol 1989;13:955-60.
5. Strauch ED, Yamaguchi J, Bass BL, Wang JY. Bile salts regulate intestinal epithelial cell migration by nuclear factor-kappa B-induced expression of transforming growth factor-beta. J Am Coll Surg 2003;197:974-84.

http://dx.doi.org/10.1016/j.jaad.2013.08.051

Angiosarcoma of the scalp successfully treated with pazopanib

To the Editor: Angiosarcoma of the scalp has one of the worst prognoses among malignant skin tumors.[1] Standard treatment guidelines for angiosarcoma do not currently exist.[1] To the best of our knowledge, this is the first case of angiosarcoma of the scalp

Fig 1. Angiosarcoma treated with pazopanib. Improvements in edema and erythema and a reduction in the size of the left cheek indurated plaque are seen following pazopanib therapy. **A**, Before pazopanib therapy. **B**, Fourteen days after the commencement of pazopanib therapy.

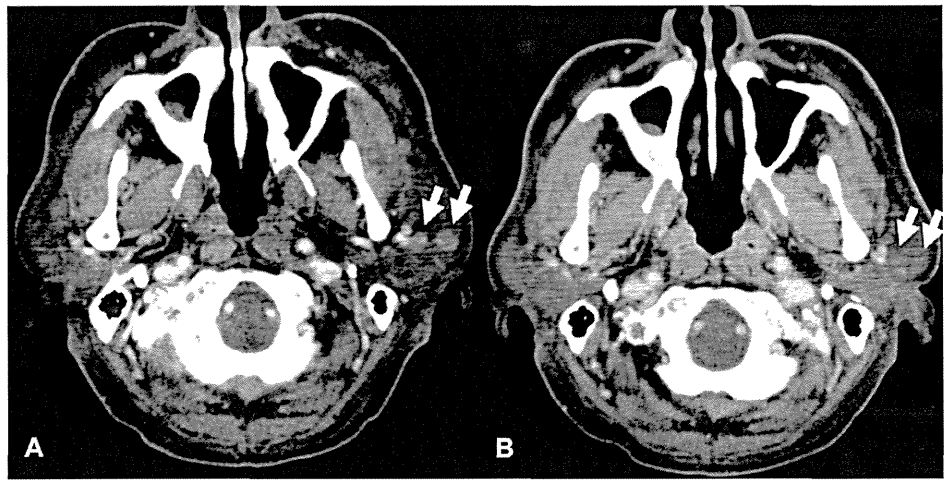

Fig 2. Angiosarcoma treated with pazopanib. Serial computed tomography scans. Scans show varying responses in multiple intraparotid lymph nodes (*arrows*). **A**, Before pazopanib therapy. **B**, Nineteen days after the commencement of pazopanib therapy.

that responded significantly to oral pazopanib administration.

A 63-year-old man presented with scalp tumors that had developed 2 months earlier. Histopathologic examination revealed atypical hyperchromatic endothelial cells, which were positive for CD31, CD34, D2-40, and VEGFR2 and which formed vascular channels. The two tumors, 60 and 20 mm in diameter, were excised with negative surgical margins; however, 4 additional surgical operations were required to remove multiple recurrences. Subsequently, weekly docetaxel (25 mg/m^2, on days 1, 8, and 15, and every 4 weeks thereafter) was administered at 8 months after initial onset; however, this treatment regimen failed to suppress the development of further cutaneous tumors. Therefore, intravenous recombinant interleukin-2 (7 × 105 U/day) combined with a 100-Gy electron

beam irradiation was administered for 11 to 18 months after onset. However, new tumors grew outside the area of irradiation. At 18 months after onset, the patient developed multiple ulcers on the scalp, a 30- × 20-mm indurated plaque on the left cheek, marked edema of the face (Fig 1, *A*), and enlargement of the involvement of multiple cervical, mandibular, and intraparotid lymph nodes (Fig 2, *A*).

Owing to the refractory nature of the tumors, pazopanib treatment was initiated at a dose of 800 mg once daily. At day 3 of pazopanib treatment, edema of the face began to subside, and the patient began to open both eyes; the edema finally disappeared by day 14. The left cheek indurated plaque completely disappeared (Fig 1, *B*). In addition, a computed tomography scan at day 19 showed shrinking of the multiple cervical, mandibular, and intraparotid lymph nodes (Fig 2, *B*). Toxic side effects of grade 3 thrombocytopenia and grade 2 neutropenia were apparent. Pazopanib therapy of 800 mg was discontinued after 2 weeks and restarted at a reduced dose of 600 mg once daily. Thereafter, the appearance of grade 3 proteinuria required that the dose be reduced further to 400 mg once daily. However, partial tumor reduction has been maintained for 26 weeks and the patient is now undergoing a pazopanib treatment without toxic side effects.

Pazopanib is a multi-targeted receptor tyrosine kinase inhibitor of VEGFR-1, VEGFR-2, VEGFR-3, PDGFR-α/β, and c-kit.[2] VEGFR-2 is up-regulated in angiosarcoma.[3] Angiosarcoma cells in the present case were also positive for VEGFR-2, suggesting that signals impinging on VEGFR-2 stimulate tumorigenesis. Accordingly, it is possible that pazopanib led to clinical improvement by inhibiting VEGFR-2 tyrosine kinase activity.

The administration of pazopanib results in rare toxic effects.[4] It is possible that taxane chemotherapy contributed to these toxic effects.

Other VEGFR inhibitors (bevacizumab, sorafenib, and sunitinib) have also been reported to be effective treatments for angiosarcoma.[1] Thus, VEGFR inhibitors, such as pazopanib, may provide an additional option for the treatment of angiosarcoma.

Hajime Tomita, MD, PhD,[a] Yuta Koike, MD, PhD,[a] Misachi Asai, MD,[a] Fumihide Ogawa, MD, PhD,[a] Kuniko Abe, MD, PhD,[b] Miki Tanioka, MD, PhD,[c] and Atsushi Utani, MD, PhD[a]

Department of Dermatology, Nagasaki University Graduate School of Biomedical Sciences[a]; Department of Pathology, Nagasaki University Hospital,[b] Nagasaki; Department of Dermatology, Kyoto University Graduate School of Medicine,[c] Kyoto

Funding sources: None.

Conflict of interest: None declared.

Correspondence to: Atsushi Utani, MD, PhD, Department of Dermatology, Nagasaki University Graduate School of Biomedical Sciences, 1-7-1 Sakamoto, Nagasaki 852-8501, Japan

E-mail: utani@nagasaki-u.ac.jp

REFERENCES

1. Young RJ, Brown NJ, Reed MW, Hughes D, Woll PJ. Angiosarcoma. Lancet Oncol 2010;11:983-91.
2. Heudel P, Cassier P, Derbel O, Dufresne A, Meeus P, Thiesse P, et al. Pazopanib for the treatment of soft-tissue sarcoma. Clin Pharmacol 2012;4:65-70.
3. Miettinen M, Rikala MS, Rys J, Lasota J, Wang ZF. Vascular endothelial growth factor receptor 2 as a marker for malignant vascular tumors and mesothelioma: an immunohistochemical study of 262 vascular endothelial and 1640 nonvascular tumors. Am J Surg Pathol 2012;36:629-39.
4. Sternberg CN, Hawkins RE, Wagstaff J, Salman P, Mardiak J, Barrios CH, et al. A randomised, double-blind phase III study of pazopanib in patients with advanced and/or metastatic renal cell carcinoma: final overall survival results and safety update. Eur J Cancer 2013;49:1287-96.

http://dx.doi.org/10.1016/j.jaad.2013.08.055

Hypersensitivity to romidepsin

To the Editor: Romidepsin is a histone deacetylase inhibitor that is FDA-approved for the treatment of refractory cutaneous T-cell lymphoma (CTCL). It is generally considered to be well tolerated, excluding previously demonstrated hematologic toxicities.[1] We report a case of a hypersensitivity reaction to romidepsin.

A 34-year-old black woman with stage IIIA CTCL diagnosed in 2010 was started on romidepsin in April 2013 for refractory disease. Previous treatments included psoralen with ultraviolet light A, extracorporeal photophoresis, interferon, bexarotene, and doxorubicin with limited to no improvement. She tolerated the first 2 cycles of romidepsin well with the initial dose administered at 10 mg/m^2 and the remaining doses at 14 mg/m^2; however, she was noted to have a low-grade fever, tachycardia, burning sensation of her skin, and headache for 24 hours following each infusion. Immediately after completion of the second 14-mg/m^2 dose of cycle 3, she became febrile to 39.5°C, tachycardic to 150 bpm, hypotensive, and erythrodermic, necessitating admission to the intensive care unit for emergent resuscitation. Following stabilization and transfer to

retardation. We treated him with oral sodium valproate. One year later, seizures had not reappeared, but his intelligence still diminished. Approximately 5 months after diagnosis, he had an operation on his right fingers, including removal of part of the bone and periosteum to prevent epiphyseal growth. One year later, his affected fingers continued to overgrow, and his right lower limb had grown 3 cm longer than the left. Therefore, the PS patient requires regular physical or imaging examinations to recognize complications and tumors, and timely operations that result in a part or complete excision of the lesion when the progressive overgrowth lead to significant loss of function.

CONFLICT OF INTEREST: None.

Zhou YANG, Zhe XU, Yu-Juan SUN, Lin MA
Department of Dermatology, Beijing Children's Hospital, Capital Medical University, Beijing, China

doi: 10.1111/1346-8138.12358

REFERENCES

1 Turner JT, Cohen MM Jr, Biesecker LG. Reassessment of the Proteus syndrome literature: application of diagnostic criteria to published cases. *Am J Med Genet A* 2004; **130**(2): 111–122.
2 Lindhurst MJ, Sapp JC, Teer JK *et al.* A mosaic activating mutation in AKT1 associated with the Proteus syndrome. *N Engl J Med* 2011; **365**: 611–619.
3 Wieland I, Tinschert S, Zenker M. High-level somatic mosaicism of AKT1 c.49G>A mutation in skin scrapings from epidermal nevi enables non-invasive molecular diagnosis in patients with Proteus syndrome. *Am J Med Genet Part A* 2013; **161A**: 889–891.
4 Barker K, Martinez A, Wang R *et al.* PTEN mutations are uncommon in Proteus syndrome. *J Med Genet* 2001; **38**: 480–481.
5 Holmes D. PI3K pathway inhibitors approach junction. *Nat Rev Drug Discov* 2011; **10**: 563–564.

Calcification of the placenta in a woman with pseudoxanthoma elasticum with a mutation of the *ABCC6* gene

Dear Editor,

A 26-year-old woman was referred to our department from an obstetrician at 12 weeks of gestation for evaluation of non-symptomatic yellowish papules on the neck and axillae, which appeared at the age of 20 years (Fig. 1a). Histological examination of a yellow papule on the right axilla showed a band of eosinophilic granular material in the dermis. Elastica van Gieson stain showed fragmentation and clumping of elastic fibers, where calcification of the degenerated fibrous components was revealed by von Kossa stain. Sequencing of the *ABCC6* gene detected a heterozygous mutation of C595T (nonsense mutation Q199X).

These skin lesions were diagnosed as pseudoxanthoma elasticum (PXE); thereafter, the other signs of PXE were screened by consulting specialists. Fundoscopic examination detected angioid streaks in both eyes, regardless of having no visual disturbance (Fig. 1b).

Electrocardiogram and echogram of the heart showed no abnormality and no calcification of large blood vessels.

At 30th week of pregnancy, a prenatal ultrasonography detected severe calcification of the placenta (Fig. 1c).

She delivered a healthy baby boy weighing 2810 g vaginally at the 39th week. The placenta (17 cm × 21 cm × 2.5 cm) weighed 640 g, and had grossly visible calcification. The calcification of vessels was evident not only in the decidua basalis (maternal side of the placenta) but also in the villus and the chorion frondosum (fetal side) (Fig. 1d–g). The umbilical arteries and vein showed slight blood congestion, but no calcification.

Pregnancy in PXE has been described to have severe complications, leading health-care providers to advise women with PXE against becoming pregnant. However, a study of 407 patients with PXE showed that it is not associated with markedly increased fetal loss or adverse reproductive outcomes.[1] On the other hand, a paper pointed out the risk on ocular lesions by labor and delivery.[2] Obstetric prognosis is dependent on the vascular damage caused by PXE. In the present case, screening examination could not find any vascular abnormalities.

The mechanism of calcification is speculated to be an abnormal function of calcium metabolism, because *ABCC6* is supposed to code a membrane transport protein.[3] Its substrate

Correspondence: Atsushi Utani, M.D., Ph.D., Department of Dermatology, Graduate School of Medicine, Nagasaki University, Nagasaki 606-8507, Japan. Email: utani@nagasaki-u.ac.jp
Author contribution: Drs Tanioka and Utani had full access to all of the data in the study and take responsibility for the integrity of the data and the accuracy of the data analysis. Study concept and design: Tamura, Kondo. Acquisition of data: Konishi, Yomisura. Analysis and interpretation of data: Utani, Tanioka, Kondo, Tamura. Drafting of the manuscript: Tanioka. Critical revision of the manuscript for important intellectual content: All authors. Statistical analysis: None. Administrative, technical, or material support: None. Study supervision: Miyachi, Konishi, Yoshimura.
Financial disclosure: None reported.
Approval: This study was approved by the local institutional review board.

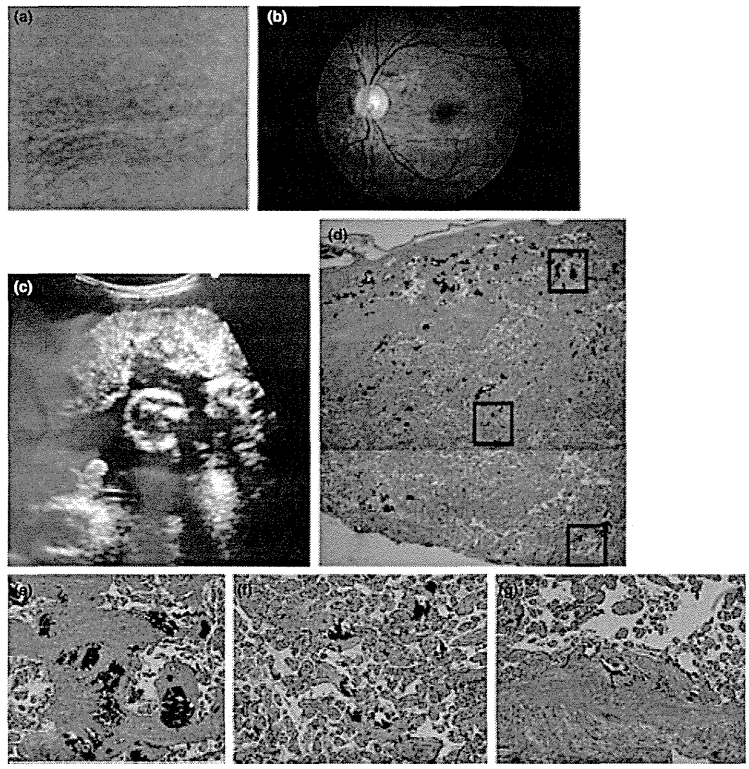

Figure 1. (a) Clinical presentation of yellow papules on the right axilla. (b) Fundus photograph of the patient's left eye. Whereas angioid streaks were observed around the optic disc and peau d'orange fundus was apparent temporal to the macula, no choroidal neovascularization was detected. (c) An echogram of the uterus at the 35th week detected calcification of the placenta. (d) Histological examination showed multiple calcified lesions in the placenta (hematoxylin–eosin [HE], ×12.5). The upper and lower parts were the fetal and maternal side of the placenta, respectively. (e) Calcification in chorion frondosum. High magnification of upper black box in (d) (fetal side) (HE, ×100). (f) Calcification in the villus. High magnification of middle black box in (d) (HE, ×100). (g) High magnification of the placenta in lower black box in (d) showed calcification of blood vessels in the decidua basalis (maternal side of the placenta) (HE, ×100).

is still unknown, but is probably an organic anion, which prevents calcification in the body. We speculated that the putative factor, which prevents calcification, is missing in patients with PXE. Q199X is the second commonest mutation in Japanese patients with PXE. Ten out of 70 Japanese patients with PXE have this nonsense mutation.

Calcification is often found in the maternal side of the mature placenta even in women with non-PXE, while villous calcification is uncommon.[4] Calcification was much more pronounced in PXE than in controls in all placental regions; maternal side, villi and fetal side.[5] Also, in the present case, the calcification was more severe in the maternal side than in the fetal side.

The diagnosis of PXE is often difficult, however, skin lesions are the first indication of PXE, which usually appears during the first and second decade of life. Dermatological evaluation of a woman with severe calcification of the placenta may lead to a diagnosis of PXE.

CONFLICT OF INTEREST: None declared.

Miki TANIOKA,[1] Atsushi UTANI,[2]
Hiroshi TAMURA,[3] Nagahisa YOSHIMURA,[3]
Norihito KASHIWAGI,[4] Eiji KONDO,[5]
Ikuo KONISHI,[5] Yoshiki MIYACHI[1]

[2]Department of Dermatology, Nagasaki University Graduate School of Medicine, Nagasaki, [1]Departments of Dermatology, [3]Ophthalmology, [4]Department of Obstetrics and Gynecology, Kashiwagi Clinic, and [5]Obstetrics and Gynecology, Kyoto University Graduate School of Medicine, Kyoto, Japan

doi: 10.1111/1346-8138.12360

REFERENCES

1 Bercovitch L, Leroux T, Terry S, Weinstock MA. Pregnancy and obstetrical outcomes in pseudoxanthoma elasticum. *Br J Dermatol* 2004; **151**: 1011–1018.
2 Farhi D, Descamps V, Picard C *et al.* Is pseudoxanthoma elasticum with severe angioid streaks an indication for Caesarean section? *J Eur Acad Dermatol Venereol* 2006; **20**: 1328–1399.